Laser-rf double-resonance study of N_2^+

N. Berrah Mansour, C. Kurtz, T. C. Steimle,* G. L. Goodman,† and L. Young
Physics Division, Argonne National Laboratory, Argonne, Illinois 60439

T. J. Scholl, S. D. Rosner, and R. A. Holt
Physics Department, The University of Western Ontario, London, Ontario, Canada N6A 3K7
(Received 4 April 1991)

We have applied the laser-rf-laser double-resonance method to a molecular ion. Fifty-six hyperfine components of fine-structure transitions ($\Delta J=\pm 1$) were measured in rotational levels from $N=1$ to 27 of the $v''=1$ vibrational level of the $X\,^2\Sigma_g^+$ ground electronic state of $^{14}N_2{}^+$. In order to fit the data, we required seven molecular constants, corresponding to the following interactions: electron spin-rotation fine structure and its centrifugal distortion, Fermi-contact hyperfine structure (hfs), dipolar hfs and its centrifugal distortion, and electric quadrupole and nuclear spin-rotation hfs. The results are in reasonable agreement with theoretical calculations based upon a Hartree-Fock-Roothaan wave function.

PACS number(s): 33.20.Bx,35.20.Sd,33.40.Ta

I. INTRODUCTION

The nitrogen molecular ion, whose optical spectrum was first observed in 1858, is one of the most thoroughly studied [1] of diatomic molecules, owing to its importance as a probe of atmospheric phenomena. However, it was only in 1982 that an optical linewidth sufficiently narrow to resolve the hyperfine structure was achieved by means of collinear ion-beam laser spectroscopy [2]. In that experiment and in a subsequent one [3], Doppler linewidths narrowed by kinematic compression [4] to between 40 and 150 MHz were observed, and the fine and hyperfine molecular constants of the (0,1) band of the $B\,^2\Sigma_u^+ \leftarrow X\,^2\Sigma_g^+$ system were measured. Optical spectroscopy provides considerably more precise information about *differences* between the molecular constants of the upper and lower electronic states than it does about the individual constants [5]; in other words, there is a strong correlation between the upper- and lower-state parameters in the fit to the data. In the present experiment we have overcome this difficulty by *direct* measurement of radio-frequency (rf) transitions in the ground electronic state.

A number of direct absorption and double resonance techniques have been developed in recent years [6]. The microwave-optical double-resonance method, in which population imbalances emerging from a source are altered by rf magnetic resonance and then probed by laser-induced fluorescence, has been demonstrated both in mass-selected beams [7] and in supersonic jets [8]. A different laser-rf double resonance method in which the optical and rf fields interact with the ions simultaneously has been applied to H_2^+ and HD^+ by Carrington and co-workers [9,10]. A stimulated resonance Raman method has recently been demonstrated [11], which allows ground-state hyperfine intervals to be measured even in situations where direct rf magnetic resonance techniques fail due to the presence of spurious signals induced by fringe-field acceleration.

The method we have applied in the present experiment has been referred to either as "laser-fluorescence molecular-beam magnetic resonance" or "laser-rf double resonance." To avoid confusion with the other double-resonance techniques we will refer to it as "laser-rf-laser double resonance" (LRL). This method, which was first demonstrated [12] with a supersonic Na_2 beam in 1975, has been described in detail elsewhere [12–17]. Briefly, a molecular-ion beam passes successively through a laser-optical-pumping region (the A region), a rf magnetic resonance region (the C region), and finally a laser-induced fluorescence probe region (the B region). In most experiments the ion beam, laser beam, and rf traveling wave are collinear, and Doppler tuning is used to ensure that the ions and the laser light are in resonance only in the A and B regions. Absorption of laser photons at A creates population differences by selectively depleting one hyperfine level of the ground electronic state. This results in a substantial decrease (~30% in the present case) in the laser-induced fluorescence monitored at the B region. rf magnetic resonance in the intervening C region can redistribute population among the fine and hyperfine levels of the ground state, detectable as an increase in laser-induced fluorescence at B. One thus has the selectivity of laser optical pumping, the sensitivity of optical photon detection, and the transit-time-limited resolution of rf resonance.

The principal aim of the present work was to obtain a very precise set of molecular constants to compare with theory. In the earlier optical study it was determined that surprisingly good agreement could be achieved between the measured molecular parameters and those calculated with Hartree-Fock-Roothaan wave functions [3]. *Ab initio* computation of wave functions and molecular parameters of simple diatomic molecules from the first row of the periodic table is a major goal of the theoretical program of chemical physics, and remains a significant index

of the maturation of this effort. Comparison with spectroscopically determined term energies, the most widely applied experimental test, is important but inadequate to probe the calculations in depth, especially in light of the fact that the wave functions are specifically optimized with respect to energy. Measurements of static parameters and transition rates with widely varying dependences on the electronic coordinates are invaluable for such tests of theory.

In the present work we report a *direct* measurement, using the LRL method, of 56 hyperfine components of fine-structure (spin-doubling) transitions for rotational states ranging from $N=1$ to 27 of the $v''=1$ vibrational level of the $X\,^2\Sigma_g^+$ ground electronic state of $^{14}N_2{}^+$. This technique represents an improvement in resolution by a factor of 500 compared to previous laser spectroscopic measurements [3]. We were able to determine seven fine- and hyperfine-structure molecular parameters with great precision, and a comparison with theory shows even closer agreement than was apparent in the relatively imprecise laser spectroscopic investigations. This will greatly facilitate the determination of the $B\,^2\Sigma_u^+$ parameters from the optical transitions being measured in a separate experiment devoted to a detailed study of perturbations arising from nearby rotational levels of the $A^2\Pi_u$ electronic state.

II. EXPERIMENTAL APPARATUS

The experiment was carried out on two completely separate apparatuses located at Argonne National Laboratory (ANL) and the University of Western Ontario (UWO). A very similar approach was taken in both laboratories but, owing to the availability of different microwave equipment, almost nonoverlapping portions of the rotational band were studied. Figure 1 shows a schematic diagram of the ANL experimental setup. This apparatus was identical to that used in a previous LRL experiment [18], except for a different ion source and a new observation region. The $N_2{}^+$ beam was produced by a rf discharge source located on an actively stabilized high-voltage platform, accelerated to 25 keV, mass analyzed in a 90° analyzing magnet, and collimated. Typical beam currents during the experiments were 0.7–1 μA. The ion beam interacted collinearly with the light beam from a frequency-stabilized cw dye laser (CR 699). The measurements required the use of Stilbene dye, which was pumped with 3 W of uv power from an argon-ion laser.

Absorption of 428-nm laser photons was used to excite $N_2{}^+$ ions in the $v''=1$ vibrational level of the $X\,^2\Sigma_g^+$ ground state to the $v'=0$ vibrational level of the $B\,^2\Sigma_u^+$ electronic state; subsequent 391-nm spontaneous emission to the $v''=0$ level of the ground state was monitored by a photon-counting photomultiplier observing the B region. This region was operated at a small postacceleration voltage (−80 V typically). This differential Doppler shift was enough to confine the laser-induced fluorescence to that region. Preliminary optical spectra were obtained by Doppler tuning the ions into resonance while scanning the laser wavelength and keeping the ion energy fixed. The laser-induced fluorescence was collected by a new optical detection system consisting of a magnetically shielded, 30-cm-long laser interaction region at the end of the beam line, described previously [19]. This device had an elliptic cross section, the interior surface being of polished aluminum with greater than 80% reflectivity down to 300 nm.

The rf was generated by a computer-controlled Adret 742A synthesizer, amplified and sent to the magnetically-

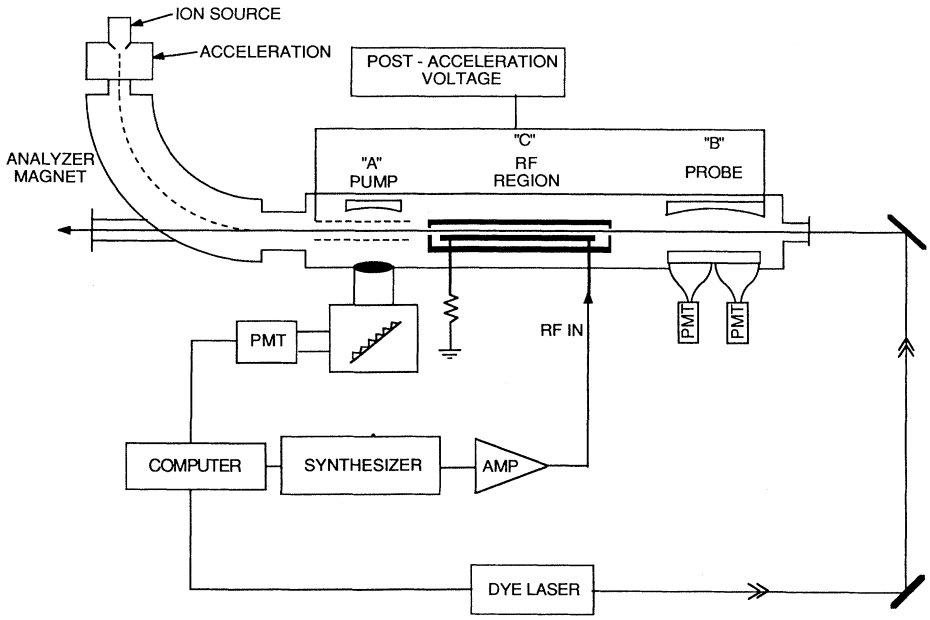

FIG. 1. Schematic diagram of the experimental apparatus used in the ANL experiment. The UWO setup was similar.

shielded C region, which has been previously described [11]. For the three rf ranges, up to 1.0 GHz, 1.0–2.0 GHz, and 2.0–4.0 GHz, the following amplifiers, respectively, were used: an AR5000 5-W amplifier, a Varian VZL-6941K1 20-W traveling-wave tube (TWT) amplifier, and a Hughes 8020H01F 20-W TWT amplifier. A LRL spectrum was accumulated by recording the fluorescence intensity in the B region as a function of the applied rf frequency.

At UWO, an ion-beam energy of 3 keV was chosen to take advantage of the narrower rf linewidth, and longer rf and optical interaction times afforded by a slow beam; the partially offsetting disadvantage is the smaller ion-beam current resulting from space-charge limitation at the lower extraction potential. The experimental setup was similar to that described previously [20], except that the rf transmission line was the one described in an earlier work [21]. The ion source was a hot-filament dc discharge Colutron [22] with a 70-μm pressure of N_2 and typically 40 mA of anode current at an anode-to-filament potential difference of 110 V. After mass selection by a Wien filter, the ion beam was brought into collinearity with a counterpropagating laser beam by means of a 5° electrostatic bend. The A and B regions were usually run with −110 V of postacceleration, although potentials from −50 to −350 V were used to ascertain that the influence of light shifts [23] was negligible. At the far end of the apparatus, a sharp electrostatic deflection directed the ion beam into a Faraday cup; typical currents into the cup were about 230 nA.

The cw laser beam at 428 nm was produced by a ring dye laser pumped by 5.7 W of uv from an argon-ion laser; typical dye-laser output power was 190 mW. To avoid long-term drifts, the dye-laser wavelength was actively stabilized to a convenient $^{130}Te_2$ absorption feature by the dc ratio method. The entire A-C-B region was maintained at 0±10 mG by three pairs of Helmholtz coils to avoid Zeeman broadening. Because the 391-nm laser-induced fluorescence at B was too intense for photon counting, an electrometer and voltage-to-frequency converter were used to transform the photomultiplier output into transistor-transistor logic (TTL) pulses that could be counted by a data acquisition board in a microcomputer.

The rf generation techniques differed for the low- and high-frequency measurements, but in both cases the reference standard was a Hewlett-Packard (HP) 8660C synthesizer under microcomputer control. For the range up to 1 GHz the direct synthesizer output was amplified by a 6-W transistor amplifier. For the 3.5–8 GHz range, an HP8620A sweeper with HP86245A and 8621A/8633A plug-ins was phase locked to a harmonic (4th to 9th) of the synthesizer output, generated in an HP934A harmonic mixer, using an HP8709A phase-lock synchronizer. The sweeper output was amplified by a 10-W Hughes 1177H06 TWT amplifier. Coaxial transmission line was chosen for the C region and the interconnections, despite the large attenuation at high frequencies, because of its broad spectral range of usefulness, the ease with which it could be coupled through the wall of the vacuum vessel, and—perhaps most importantly—the absence of frequency-dependent Doppler shifts for TEM-mode waves. We did in fact observe additional resonance signals from the TE_{11} coaxial waveguide mode; these are discussed in Appendix A.

III. PROCEDURE

The transitions of the $B\,^2\Sigma_u^+ \leftarrow X\,^2\Sigma_g^+$ (0,1) band that we employed for optical pumping were mostly P-branch transitions ($\Delta J=-1$) but a few R-branch lines ($\Delta J=+1$) were also used. The nuclear spin I_1 of ^{14}N is 1, giving rise to a total nuclear spin $I=0,1,2$ in $^{14}N_2{}^+$. The Pauli principle for identical bosons allows only $I=1$ for odd N and $I=0,2$ for even N. Figure 2 shows energy-level diagrams for odd and even N, with the principal P-branch optical transitions indicated. The fine-structure (electronic spin-rotation) interaction causes spin doubling: the total electronic angular momentum can be either $J=N-\frac{1}{2}$ or $J=N+\frac{1}{2}$. The hyperfine interactions split each of these into three levels for $I=1$ and six levels for $I=0,2$; these interactions have matrix elements that are off diagonal in J, which cause noticeable distortions of the hyperfine spacing, especially for low N, where the spin-doubling interval is small. A typical optical spectrum, obtained by scanning the laser wavelength while observing the B fluorescence (with the A region at ground potential), is shown in Fig. 3. The ≈120-MHz full width at half maximum (FWHM) linewidth is mainly due to ion energy spread. The $F=J$ lines due to $I=0$ and $I=2$ are not optically resolvable and give rise to the peaks of double height. Although both I levels are thus optically pumped, the corresponding LRL signals are distinct.

As mentioned in the Introduction, direct measurement of "pure hyperfine" transitions ($\Delta J=0$, $\Delta F=\pm1$) that occur at low radio frequency is not possible in this case because of interfering signals from ion acceleration in the fringing fields of the C region [11]. In addition, the small size of the nuclear magneton imposes unacceptable rf power requirements. For these reasons, all the measurements were of fine-structure transitions ($\Delta J=\pm1$, $\Delta F=0,\pm1$). Transitions of this type involve "flipping" an electron spin and thus are characterized by strong transition probabilities due to the large size of the Bohr magneton. The principal lines, which satisfy $\Delta F=\Delta J$, are indicated in Fig. 2. In a few cases at low N we were able to measure satellite transitions ($\Delta F \neq \Delta J$). The rf power was typically 3 W at ANL and 3.5–10 W at UWO. Drifts of the ion-beam energy are a source of possible systematic error via the rf Doppler shift; thus, we made measurements with the rf propagation direction parallel and antiparallel to the ion-beam velocity in rapid succession.

In the measurements at UWO above 3.5 GHz we could record resonance signals from both propagation directions in the same spectrum by leaving the rf transmission line unterminated and interposing a coaxial ferrite isolator to protect the TWT amplifier. The scanning program stepped the rf frequency and recorded the B-region laser-induced fluorescence signal as well as the rf power, laser power, and ion-beam current. The rf power was sampled by means of a directional coupler inserted between

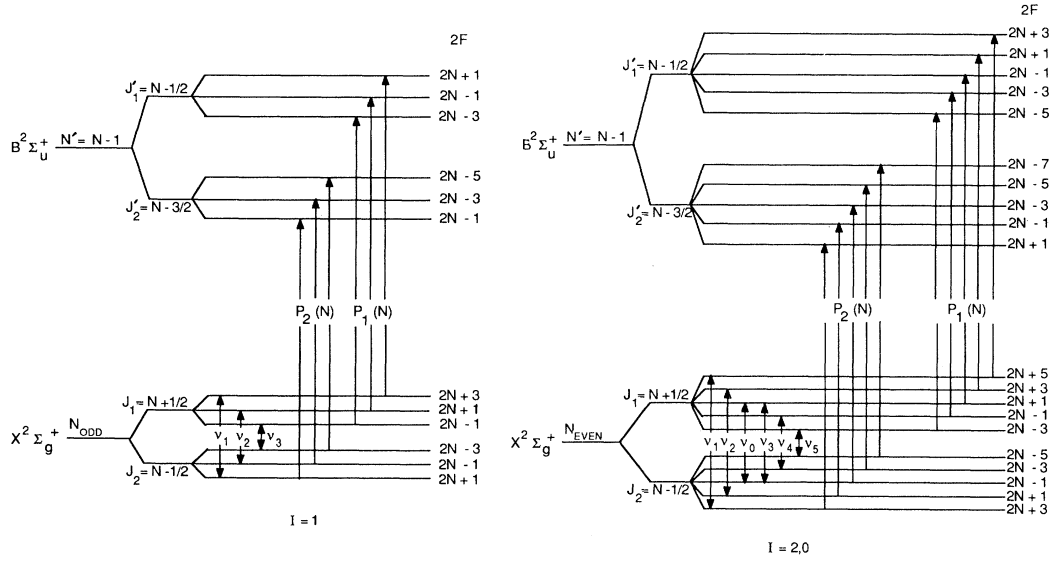

FIG. 2. Energy-level diagram for typical even-N and odd-N rotational levels of the $X^2\Sigma_g^+$ state of $^{14}N_2^+$, showing the principal P-branch optical pumping transitions to the $B^2\Sigma_u^+$ electronically excited state, $P_1(N)$ and $P_2(N)$, as well as the principal transitions in the laser-rf-laser double-resonance (LRL) experiment, $\nu_0, \ldots, \nu_5$. Note that the $I=0$, $F=J$ levels are not shown, but lie close to the $I=2$, $F=J$ levels.

the isolator and the transmission line. Below 1 GHz the power was measured at the 50Ω termination of the line. Many short up-and-down scans, each lasting about 10 sec, were used rather than one scan of longer duration, in order to avoid systematic error from drifts.

IV. RESULTS AND INTERPRETATION

Typical low- and high-frequency LRL spectra are shown in Fig. 4. Each resonance peak was fitted to a Rabi two-level formula [24, 25] plus a background,

$$R(\omega;\omega_o,\omega_R,A,B) = A\frac{\omega_R^2}{(\omega_o-\omega)^2+\omega_R^2}\sin^2\{\tfrac{1}{2}[(\omega_o-\omega)^2+\omega_R^2]^{1/2}t\}+B,$$

where ω_o, ω_R, A, and B are adjustable parameters to be fitted and t is the known time of flight in the C region. Although the actual signal ought to be a sum of such functions with varying Rabi frequencies ω_R, this has no effect on the determination of the line center. The FWHM linewidths were typically 600–900 kHz for the ANL data and 200 kHz for the UWO data (owing to the slower ion velocity). For each transition we determined the resonance frequency taken with the rf propagation direction parallel and antiparallel to the ion velocity. The geometric mean of these two measurements then yielded a transition frequency that is Doppler-free to all orders. The results of all measurements are presented in Table I.

The Hamiltonian used for the interpretation of the data included all interactions whose coupling constants could be determined from least-squares fitting and that were found to lower the χ^2 significantly. Since only a single vibrational level was studied, the constants are specific to the $v''=1$ level. The complete Hamiltonian is [26, 27]

$$H = H_{\gamma,\gamma_N} + H_{b_F} + H_{t,t_N} + H_{eqQ} + H_{c_I}.$$

The H_{γ,γ_N} term is the electronic spin-rotation interaction responsible for the $J=N\pm S$ fine structure. In $^2\Sigma$ states, the true spin-rotation coupling constant is very small, and the effective constant represents second-order effects from spin-orbit and rotation-electronic coupling to nearby $^2\Pi$ states. The effective operator is [28–30]

$$H_{\gamma,\gamma_N} = [\gamma+\gamma_N N(N+1)]\mathbf{N}\cdot\mathbf{S}.$$

We follow the convention of Childs *et al.* [31] to describe the centrifugal distortion.

The matrix elements of all the relevant hyperfine interactions are well known in the molecular bases corresponding to the usual Hund cases. For a diatomic molecule in a Σ state, Hund's case b_{β_J} is convenient, and the matrix elements for the case where only one nucleus has a spin I_1 are given by Bowater, Brown, and Carrington [32]. It is worth noting that the formulas for the more general case of a homonuclear diatomic molecule with total nuclear spin I cannot be generated by simply replacing I_1 by I in the hyperfine Hamiltonian and omitting the sum over both nuclei [33]. While this replacement does actually

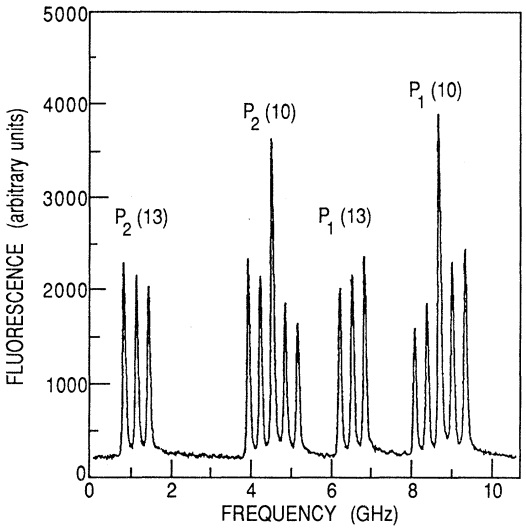

FIG. 3. An ion-beam laser-fluorescence spectrum near the bandhead of the $B^2\Sigma_u^+ \leftarrow X^2\Sigma_g^+$ (0,1) band, obtained by scanning the frequency of a cw dye laser while recording laser-induced fluorescence from a region in which the laser beam overlaps the N_2^+ ion beam collinearly.

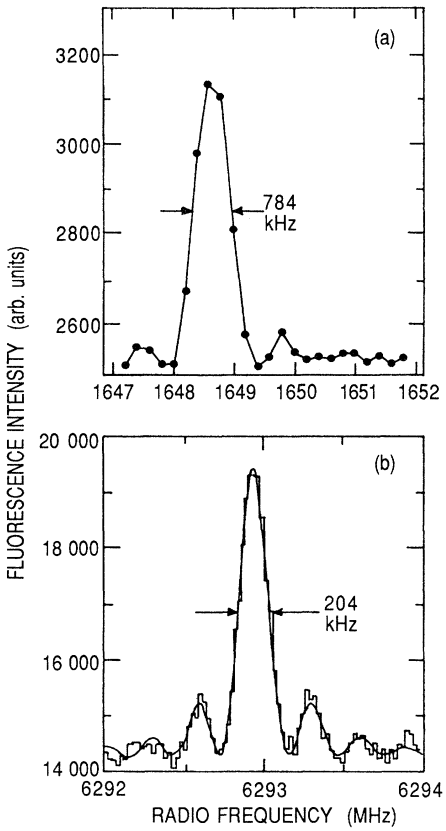

FIG. 4. Typical LRL spectra of fine-structure transitions ($\Delta J=\pm1$) in the $v''=1$ level of the $X^2\Sigma_g^+$ ground state of $^{14}N_2^+$. (a) Spectrum of the $J=5.5$, $F=3.5\leftrightarrow J=6.5$, $F=4.5$ transition measured at ANL. (b) Spectrum of the $J=21.5$, $F=22.5\leftrightarrow J=22.5$, $F=23.5$ transition measured at UWO. The secondary, off-resonance peaks are as predicted by the theoretical Rabi line shape.

work for the Fermi-contact and magnetic dipolar interactions, it fails for the electric quadrupole interaction, where matrix elements off diagonal in I exist. We have generalized all the relevant formulas of Bowater, Brown, and Carrington [32] to the homonuclear case; details of this calculation for the electric quadrupole case are given in Appendix B.

The matrix elements of the Fermi-contact hyperfine Hamiltonian are [32]

$$\langle N',S',J',I',F',M_F'|H_{b_F}|N,S,J,I,F,M_F\rangle$$
$$= b_F\delta_{N'N}\delta_{S'S}\delta_{I'I}\delta_{F'F}\delta_{M_F'M_F}(-1)^{F+I+J'+J+N+S+1}[I(I+1)(2I+1)]^{1/2}$$
$$\times[S(S+1)(2S+1)(2J+1)(2J'+1)]^{1/2}\begin{Bmatrix} I & J' & F \\ J & I & 1 \end{Bmatrix}\begin{Bmatrix} S & J' & N \\ J & S & 1 \end{Bmatrix}.$$

This interaction has matrix elements satisfying $\Delta J = 0,\pm1$ and thus mixes states of the same F belonging to the upper and lower levels of the spin doublet. In this, and equations that follow, the curly brackets signify six- and nine-j symbols and the parentheses three-j symbols.

The matrix elements of the dipolar hyperfine interaction are [32]

$$\langle N',S',J',I',F',M_F'|H_{t,t_N}|N,S,J,I,F,M_F\rangle$$
$$= [t+t_N N(N+1)]\delta_{S'S}\delta_{I'I}\delta_{F'F}\delta_{M_F'M_F}(-1)^{J+I+F+N'+1}[30I(I+1)(2I+1)S(S+1)(2S+1)]^{1/2}$$
$$\times[(2J+1)(2J'+1)(2N+1)(2N'+1)]^{1/2}\begin{Bmatrix} I & J' & F \\ J & I & 1 \end{Bmatrix}\begin{Bmatrix} N' & N & 2 \\ S & S & 1 \\ J' & J & 1 \end{Bmatrix}\begin{pmatrix} N' & 2 & N \\ 0 & 0 & 0 \end{pmatrix}.$$

This interaction has off-diagonal matrix elements satisfying $\Delta J = 0,\pm1$ and $\Delta N = 0,\pm2$.

The electric quadrupole interaction obeys the selection rules ΔJ=0, ±1,±2, ΔI=0,±2, and ΔN=0,±2, allowing for quite a few off-diagonal matrix elements. These not only affect the pattern of energy-level spacings but also make it possible to observe $\Delta I=\pm2$ transitions as a result of the mixing of the eigenstates of total nuclear spin. The matrix

TABLE I. $^{14}N_2^+$ ($v''=1$) $\Delta J=\pm 1$ transition frequencies (in MHz).

N	I	F	F'	Source	Frequency	Error	Fit	Residual
1	1	0.5	0.5	UWO	361.866	0.011	361.866	0.000
	1	0.5	1.5	UWO	416.043	0.009	416.040	0.003
	1	1.5	1.5	UWO	419.748	0.011	419.748	0.000
	1	1.5	2.5	UWO	476.222	0.009	476.219	0.003
2	2	0.5	0.5	UWO	545.836	0.009	545.834	0.002
	2	0.5	1.5	UWO	584.195	0.009	584.193	0.002
	2	1.5	1.5	UWO	610.000	0.010	609.997	0.003
	2	1.5	2.5	UWO	662.259	0.009	662.262	−0.003
	2	2.5	2.5	UWO	693.961	0.009	693.963	−0.002
	2	2.5	3.5	UWO	749.967	0.009	749.973	−0.006
	2	3.5	3.5	UWO	777.884	0.012	777.882	0.002
	2	3.5	4.5	UWO	828.496	0.009	828.495	0.001
	0	1.5	2.5	UWO	692.315	0.009	692.311	0.004
3	1	1.5	2.5	ANL	894.733	0.009	894.740	−0.007
	1	2.5	3.5	ANL	962.832	0.014	962.829	0.003
	1	2.5	3.5	UWO	962.830	0.009	962.829	0.001
	1	3.5	3.5	UWO	991.793	0.010	991.793	0.000
	1	3.5	4.5	ANL	1037.299	0.011	1037.301	−0.002
	1	3.5	4.5	UWO	1037.304	0.009	1037.301	0.003
4	2	2.5	3.5	ANL	1156.829	0.012	1156.825	0.004
	2	3.5	4.5	ANL	1229.442	0.019	1229.434	0.008
	2	4.5	5.5	ANL	1307.574	0.013	1307.566	0.008
	2	5.5	6.5	ANL	1385.853	0.006	1385.855	−0.002
	0	3.5	4.5	ANL	1246.127	0.023	1246.131	−0.004
5	1	3.5	4.5	ANL	1448.849	0.005	1448.848	0.001
	1	4.5	5.5	ANL	1518.664	0.014	1518.658	0.006
	1	5.5	6.5	ANL	1592.820	0.007	1592.818	0.002
6	2	3.5	4.5	ANL	1650.977	0.013	1650.971	0.006
	2	4.5	5.5	ANL	1716.476	0.007	1716.478	−0.002
	2	5.5	6.5	ANL	1788.346	0.012	1788.350	−0.004
	2	6.5	7.5	ANL	1864.086	0.009	1864.083	0.003
	2	7.5	8.5	ANL	1941.106	0.006	1941.106	0.000
7	1	5.5	6.5	ANL	2002.935	0.023	2002.937	−0.002
	1	6.5	7.5	ANL	2073.481	0.032	2073.500	−0.019
	1	7.5	8.5	ANL	2147.310	0.010	2147.315	−0.005
8	2	7.5	8.5	ANL	2344.780	0.034	2344.770	0.010
	2	6.5	7.5	ANL	2273.030	0.023	2273.039	−0.009
	2	5.5	6.5	ANL	2205.689	0.024	2205.689	0.000
	0	7.5	8.5	ANL	2353.626	0.033	2353.627	−0.001
13	1	11.5	12.5	UWO	3664.212	0.009	3664.205	0.007
	1	12.5	13.5	UWO	3735.660	0.009	3735.643	0.017
14	2	11.5	12.5	UWO	3867.540	0.009	3867.547	−0.007
	2	12.5	13.5	UWO	3937.164	0.009	3937.168	−0.004
	2	13.5	14.5	UWO	4008.961	0.009	4008.962	−0.001
	2	14.5	15.5	UWO	4082.565	0.009	4082.569	−0.004
	2	15.5	16.5	UWO	4157.346	0.009	4157.344	0.002
	0	13.5	14.5	UWO	4014.211	0.009	4014.213	−0.002
22	2	19.5	20.5	UWO	6080.197	0.009	6080.206	−0.009
	2	21.5	22.5	UWO	6222.829	0.009	6222.830	−0.001
	0	21.5	22.5	UWO	6226.300	0.009	6226.301	−0.001

TABLE I. (*Continued*).

N	I	F	F'	Source	Frequency	Error	Fit	Residual
23	1	21.5	22.5	UWO	6429.562	0.009	6429.561	0.001
	1	23.5	24.5	UWO	6574.414	0.009	6574.416	−0.002
	1	22.5	23.5	UWO	6501.454	0.009	6501.460	−0.006
25	1	23.5	24.5	UWO	6982.015	0.009	6982.003	0.012
	1	25.5	26.5	UWO	7126.879	0.009	7126.880	−0.001
27	1	25.5	26.5	UWO	7534.199	0.009	7534.196	0.003
	1	26.5	27.5	UWO	7606.190	0.009	7606.192	−0.002
	1	27.5	28.5	UWO	7679.094	0.009	7679.093	0.001

elements are

$$\langle N', S', J', I', F', M_F' | H_{eqQ} | N, S, J, I, F, M_F \rangle$$

$$= \frac{eqQ}{2} \delta_{S'S} \delta_{F'F} \delta_{M_F' M_F} \frac{(-1)^I + (-1)^{I'}}{2} [(2I+1)(2I'+1)(2J+1)(2J'+1)(2N+1)(2N'+1)]^{1/2} (-1)^{F+2J+I'}$$
$$\times (-1)^{2I_1+S+2N'} \begin{Bmatrix} I' & 2 & I \\ J & F & J' \end{Bmatrix} \begin{Bmatrix} I_1 & 2 & I_1 \\ I & I_1 & I' \end{Bmatrix} \begin{Bmatrix} N' & 2 & N \\ J & S & J' \end{Bmatrix} \begin{pmatrix} N' & 2 & N \\ 0 & 0 & 0 \end{pmatrix} \begin{pmatrix} I_1 & 2 & I_1 \\ -I_1 & 0 & I_1 \end{pmatrix}^{-1},$$

as shown in Appendix B.

Finally, the magnetic nuclear spin-rotation interaction $H_{c_I} = c_I \mathbf{I} \cdot \mathbf{N}$ has matrix elements [27]

$$\langle N', S', J', I', F', M_F' | H_{c_I} | N, S, J, I, F, M_F \rangle$$

$$= c_I \delta_{N'N} \delta_{S'S} \delta_{I'I} \delta_{F'F} \delta_{M_F' M_F}$$
$$\times (-1)^{F+I+J'+J+N+S+1} [I(I+1)(2I+1)N(N+1)(2N+1)(2J+1)(2J'+1)]^{1/2} \begin{Bmatrix} J & 1 & J' \\ I & F & I \end{Bmatrix} \begin{Bmatrix} N & 1 & N \\ J' & S & J \end{Bmatrix}.$$

The predicted frequencies for a set of molecular parameters were calculated by direct diagonalization of the complete Hamiltonian, which is diagonal in F and thus block diagonal. In general, for each value of F, the block contains values of I, J, and N satisfying $\Delta I = 0, \pm 2$, $\Delta J = 0, \pm 1, \pm 2$, and $\Delta N = 0, \pm 2$. In practice, we found that the effect of including mixing with nearby rotational levels was negligible even at low N, and so we omitted it from the fit. A standard nonlinear least-squares minimization routine [34] was used to fit the seven fine- and hyperfine-structure parameters to the data.

In order to provide a check of the analysis outlined above, which generalized the Hamiltonian for a single nuclear spin, the data were analyzed independently using the standard spin Hamiltonian for a diatomic $^2\Sigma$ radical with two nonzero nuclear moments, I_1 and I_2. The matrix elements of the hyperfine interaction are given by Ryzlewicz *et al.* [35] in their Table I and are not reproduced here. They are correct as shown, except for an obvious misprint in the first line where $\langle \| I_2 \| \rangle$ should be $\langle \| I_1 \| \rangle$. Here it is noted that the previously introduced dipolar parameter t is equivalent to $c/3$, where c is the Frosch-Foley dipolar parameter used by Ryzlewicz *et al.* For the homonuclear diatomic radical N_2^+ it is more convenient to use the $|N, S, J, (I_1, I_2) I, F\rangle$ basis states than the basis set $|N, S, J, I_1, F_1, I_2, F\rangle$ used by Ryzlewicz. The transformation for an arbitrary operator X is

$$\langle N, S, J, (I_1 I_2) I, F, M_F | X | N, S, J', (I_1 I_2) I', F, M_F \rangle$$

$$= \sum_{F_1, F_1'} (-1)^{J-J'} [(2I+1)(2I'+1)(2F_1+1)(2F_1'+1)]^{1/2} \begin{Bmatrix} J & I_1 & F_1 \\ I_2 & F & I \end{Bmatrix} \begin{Bmatrix} J' & I_1 & F_1' \\ I_2 & F & I' \end{Bmatrix}$$
$$\times \langle N, S, J, I_1, F_1, I_2, F, M_F | X | N, S, J', I_1, F_1', I_2, F, M_F \rangle.$$

The resulting expressions for the matrix elements were used to calculate energy levels for a given set of molecular parameters by direct diagonalization. The calculation includes interactions between states of total nuclear spin $I = 0$ and 2. However, it was found to be unnecessary to include interactions between states with different rotational quantum numbers N. The effect of neglecting such interactions should be most pronounced at low N where the energy separations are the smallest. The quality of the fits reveals no systematic degradation at low N; thus, these interactions are not important at this level of precision. The appropriate energy levels were then selected to calculate the observed rf transitions. This input was then used in a standard least-squares-fitting program, E04FCF of the Numerical Algorithms Group (NAG) Library Service, to produce a fit of the seven fine- and hyperfine-structure parameters previously mentioned to the data.

The transition frequencies calculated by both analysis programs agree perfectly. The fitted transition frequencies are compared with the data in Table I. The agreement is excellent, with a χ^2/DF of 0.26. At the high-frequency end of the data, the precision with which the transition frequencies have been determined reaches 1 ppm.

It is interesting to note the relative merit of using the tensor form to express the dipolar hyperfine interaction compared to the $I_z S_z$ form of Frosch and Foley [26]. Using the Frosch and Foley parametrization, eight parameters, rather than seven, were required to fit the data to the same level of precision. The extra parameter required is b_N, the centrifugal distortion of the b parameter. This need arises because, although the Fermi contact interaction changes very little with internuclear separation, the b parameter ($b = b_F - t$) changes significantly. This shows the clear advantage of using the tensor form.

Table II lists the fitted molecular constants (appropriate for an individual nitrogen nucleus) as well as those from previous optical measurements by Gottscho *et al.* [36], Miller, Suzuki, and Hirota [37], and Rosner, Gaily, and Holt [3]. Several interaction constants are measured for the first time, including eqQ; and all are determined with much greater precision. Not listed in the table is a related measurement of b_F (equivalent to A_{iso}) for the $v''=0$ level of $^{14}N_2^+$ done by ESR techniques in a neon matrix by Knight and co-workers [38]. Their value of b_F=104.1(6) MHz for the ground vibrational level in $^{14}N_2^+$ is very similar to our current value for the first excited level. Since the dependence of b_F on v is expected to be small (measured [39] as a 2.4% decrease between $v=0$ and 1 for the isoelectronic CN), this comparison reaffirms the typical small gas phase to matrix shift [40].

In Table II we also list a value of γ estimated by Gottscho *et al.* [36] and hyperfine constants calculated by Rosner, Gaily, and Holt [2] from the Hartree-Fock-Roothaan (HFR) wave function of Cade, Sales, and Wahl [41]. The restricted-HFR wave function used decribes the single dominant molecular-orbital configuration for the $X\,^2\Sigma_g^+$ state of $^{14}N_2^+$, namely,

$$1\sigma_g^2 1\sigma_u^2 2\sigma_g^2 2\sigma_u^2 3\sigma_g^1 1\pi_u^4,$$

in terms of Slater-type orbitals. Using this simple description of the molecular orbital (and the value [42] μ=0.4073 nm for ^{14}N), values for the Fermi-contact and dipolar interactions were calculated. The b_F parameter differs from the experimental value by $\approx$9%, and the t by only $\approx$4%. Even better agreement, such as that obtained for the N atom [43], can be expected with the use of improved wave functions and considerably greater computational effort [44–46].

The measured hyperfine parameters b_F, t, and eqQ are useful in developing a qualitative picture of the molecular-orbital structure in the $X\,^2\Sigma_g^+$ state of $^{14}N_2^+$. These parameters are related to various electronic integrals as follows [26, 40]:

$$b_F = \frac{8\pi}{3} g_e g_N \mu_B \mu_N \langle \delta(r) \rangle_{av},$$

$$t = \frac{1}{2} g_e g_N \mu_B \mu_N \left\langle \frac{(3\cos^2\theta - 1)}{r^3} \right\rangle_{av},$$

$$eqQ = e^2 Q \left\langle \frac{\sum_i (3\cos^2\theta_i - 1)}{r^3} \right\rangle_{av},$$

TABLE II. Fine and hyperfine constants of the $X\,^2\Sigma_g^+$ ($v''=1$) level of $^{14}N_2^+$.

Parameter	Theory (MHz)	Experiment (MHz) Present work	Gottscho *et al.*[a]	Miller, Suzuki, and Hirota[b]	Rosner, Gaily, and Holt[c]
γ	<360[a]	276.92253(13)	270(150)	259(7)	279.1(6)
γ_N		$-3.9790(23)\times10^{-4}$			
b_F	91[d]	100.6040(15)			105(4)
t	27[d]	28.1946(13)			49(6)
t_N		$-7.35(27)\times10^{-5}$			
eqQ		0.7079(60)			
c_I		0.01132(85)			

[a] Reference [36].
[b] Reference [37].
[c] Reference [3].
[d] Reference [2].

where g_e and g_N are the electron and nuclear g factors respectively, μ_B and μ_N are the Bohr and nuclear magnetons, and Q is the nuclear quadrupole moment. The averages in b_F and t are over all electrons contributing to the spin angular momentum; in contrast, the sum in eqQ is over all electrons, including those in core orbitals.

The Fermi-contact parameter b_F is traditionally used as a measure of atomic s-orbital contribution to the molecular orbital of the unpaired electron. This can be approximated by taking the ratio of the measured b_F to that for the N atomic $2s$ orbital (1811 MHz) [47]. For the $3\sigma_g$ orbital under consideration, this yields $\approx 6\%$ s character. This is in good agreement with the naive notion that the $3\sigma_g$ orbital is bonding, with primarily $2p_z$ character. Here we note that a qualitative look at the coefficients in the expansion for the $3\sigma_g$ orbital is misleading in the determination of percentage s character in the case of the Cade *et al.* wave functions. This is due to the fact that the Slater-type s orbitals used in the basis set have nodes at the nucleus for all $n \geq 2$. A more accurate method to derive this quantity theoretically is to calculate the overlap between the optimized wave function and an appropriate atomic orbital [48].

The dipolar parameter t derived from the HFR wave function is in even better agreement with experiment than the b_F. This is not surprising in that either polarization of the core or a small admixture of configurations containing three open shells could vastly alter the observed b_F. Neither possibility is allowed in the Cade *et al.* wave function.

A comparison between the eqQ and t parameters shows a substantial amount of core polarization occurring in this system. The contribution to the electric-field gradient at the ^{14}N nucleus originating from the unpaired $3\sigma_g$ electron alone can be deduced from the value of t. The angular average $\langle(3\cos^2\theta - 1)/r^3\rangle_{\rm av}$ arising from the unpaired $3\sigma_g$ electron can be computed from the formula for t assuming $g_e = 2.0$ and $\mu_n = 0.403\,75$ nm. Combining this with the value of $Q = 0.01$ b [42], the contribution to eqQ from this single electron is found to be -3.4 MHz. This is considerably different from the measured value of 0.708 MHz, which includes contributions from the closed shells. The closed π and σ shells are evidently distorted. This is true to a lesser extent in the isoelectronic CN molecule, where the measured [39] eqQ, -1.307 MHz, is more nearly equal to that predicted to arise solely from the unpaired electron, -2.4 MHz.

V. CONCLUSION

We have applied the laser-rf-laser double-resonance method to a molecular ion, $^{14}N_2{}^+$. Using this technique, we have measured seven fine and hyperfine interaction constants with unprecedented precision. The Fermi-contact and dipolar parameters are calculated to within 10% using a simple single-configuration Hartree-Fock-Roothaan wave function. It is hoped that these measurements will serve as an important benchmark for future computations.

ACKNOWLEDGMENTS

N.B.N., C.K., T.C.S., G.L.G., and L.Y. wish to thank W. J. Childs for his valuable comments and numerous discussions and T. P. Dinneen for help with preliminary optical measurements. In addition, we thank J. Delayen and C. Roche for the loan of the TWT amplifiers. This research was supported by the U.S. Department of Energy, Office of Basic Energy Science, under Contract No. W-31-109-ENG-38. T.J.S., S.D.R., and R.H. wish to acknowledge the financial support of the Natural Sciences and Engineering Research Council of Canada and the Centre of Excellence in Molecular and Interfacial Dynamics (CEMAID).

APPENDIX A: WAVEGUIDE MODES

The spectra in the 6–8 GHz region show additional rf resonance signals which can be readily interpreted as due to TE_{11} waveguide modes. Figure 5 shows a typical example in which there are four resonances from the copropagating and counterpropagating TEM and TE_{11} waves. Although coaxial transmission lines can propagate transverse waves of any frequency, the Ohmic losses associated with current flow, especially in the center conductor, become severe at high frequencies. The waveguide modes, in which either the **E** and **H** field has a longitudinal (z) component, have much lower losses but can only propagate above characteristic cutoff frequencies.

The theory of guided wave propagation is well known [49]. The longitudinal magnetic field of a coaxial TE_{nm}

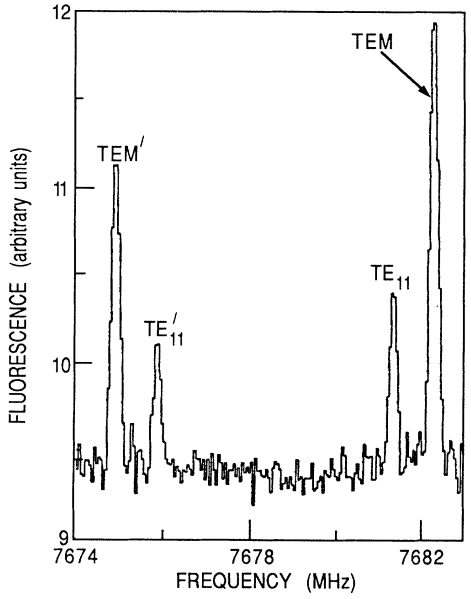

FIG. 5. LRL spectrum of the J=26.5, F=27.5↔J=27.5, F=28.5 transition, showing the TEM and TE_{11} resonances for both copropagating (unprimed) and counterpropagating (primed) rf traveling waves.

waveguide mode is

$$H_z(r,\phi) = [AJ_n(k_c r) + BY_n(k_c r)]\cos(n\phi + \delta) \times \exp[i(k_g z - \omega t)],$$

where J_n and Y_n are Bessel functions, δ specifies the polarization, and ω is the angular frequency. The cutoff wave number k_c of the TE_{nm} mode is the mth root of

$$Y_n'(k_c a)J_n'(k_c b) - Y_n'(k_c b)J_n'(k_c a) = 0,$$

which comes from applying the boundary condition $\partial H_z/\partial r=0$ at the inner ($r=a$) and outer ($r=b$) walls. A similar formula, with the Bessel functions themselves rather than their derivatives, yields the cutoff wave numbers of the TM_{nm} modes. The TE_{11} cutoff frequency $f_c=(c/2\pi)k_c$ calculated from the dimensions of our coaxial line, a=5.65±0.06 mm, b=13.02±0.06 mm, is 5218±37 MHz. All other modes have $f_c > 10$ GHz.

The wave number in the guide, k_g, is related to the free-space wave number $k=\omega/c$ according to

$$k_g = 2\pi/\lambda_g = (k^2 - k_c^2)^{1/2}.$$

From the exponential factor in H_z we obtain the phase velocity

$$v_p = \omega/k_g = (k/k_g)c = (\lambda_g/\lambda)c.$$

The Doppler-shifted frequency detected by an ion moving with velocity $\pm v$ in the z direction is the inverse of the time between encounters with wave fronts of equal phase,

$$\nu' = (v_p \pm v)/\lambda_g = \nu[1 \pm (\lambda/\lambda_g)(v/c)],$$

which is the standard nonrelativistic Doppler formula with

$$\beta' = (\lambda/\lambda_g)\beta = [1 - (k_c/k)^2]^{1/2}\beta.$$

Figure 6 shows that the values of β'/β calculated from this formula *with no adjustable constants* are in excellent agreement with those obtained from the intervals between resonance peaks in the spectra.

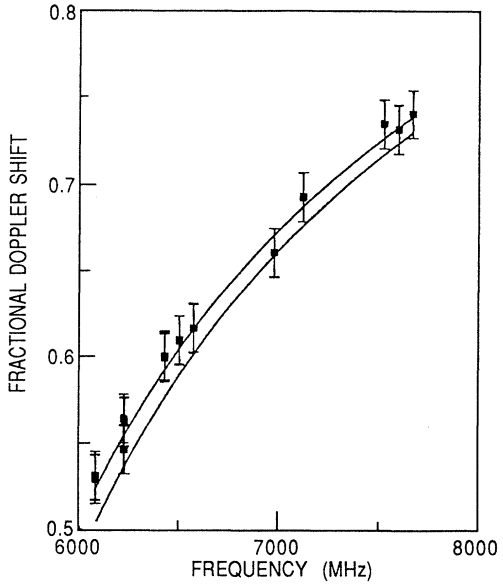

FIG. 6. Ratio of TE_{11} Doppler shift to TEM Doppler shift vs rf frequency. The solid lines indicate the theoretical prediction, with no adjustable constants, for the maximum and minimum values of the transmission line dimensions allowed by normal machining tolerances (±0.005″=±0.013 cm).

APPENDIX B: ELECTRIC QUADRUPOLE MATRIX ELEMENTS

In this section we outline the derivation of the matrix elements of the electric quadrupole interaction in a homonuclear diatomic molecule. Using spherical tensor notation, the Hamiltonian can be written as [32]

$$H_{eqQ} = e\sum_{i=1,2} T^{(2)}(Q_i)T^{(2)}(\nabla \cdot \mathbf{E}_i),$$

where the sum extends over both nuclei. A general matrix element of H_{eqQ} in a Hund case $b_{\beta J}$ basis can then be evaluated using a standard formula from irreducible tensor analysis [50] as

$$\langle N', S', J', (I_1, I_2)I', F', M_F'|H_{eqQ}|N, S, J, (I_1, I_2)I, F, M_F\rangle$$

$$= e\delta_{S'S}\delta_{F'F}\delta_{M_F'M_F}(-1)^{F+I'+J}\begin{Bmatrix} I' & 2 & I \\ J & F & J' \end{Bmatrix}\sum_{i=1,2}\langle N', S', J'||T^{(2)}(\nabla \cdot \mathbf{E}_i)||N, S, J\rangle\langle I_1, I_2, I'||T^{(2)}(Q_i)||I_1, I_2, I\rangle.$$

The reduced matrix elements may be further reduced by another standard formula [50] according to

$$\langle I_1, I_2, I'||T^{(2)}(Q_1)||I_1, I_2, I\rangle = (-1)^{I+I_1+I_2}[(2I+1)(2I'+1)]^{1/2}\begin{Bmatrix} I_1 & 2 & I_1 \\ I & I_2 & I' \end{Bmatrix}\langle I_1||T^{(2)}(Q_1)||I_1\rangle,$$

with a similar formula for the other nucleus, in which the indices 1 and 2 are interchanged on the right-hand side and $(-1)^I$ is replaced by $(-1)^{I'}$ (leading to cancellation of the two terms when $I + I'$ is odd). For two identical nuclei in equivalent molecular sites, $I_1=I_2$, $T^{(2)}(Q_1)=T^{(2)}(Q_2)$, and $T^{(2)}(\nabla \cdot \mathbf{E}_1)=T^{(2)}(\nabla \cdot \mathbf{E}_2)$. The conventional definition of the electric quadrupole moment is [25]

$$Q = Q_2 = Q_1 \equiv 2\langle I_1, I_1, I|T_0^{(2)}(Q_1)|I_1, I_1, I\rangle = 2\langle I_1||T^{(2)}(Q_1)||I_1\rangle \begin{pmatrix} I_1 & 2 & I_1 \\ -I_1 & 0 & I_1 \end{pmatrix}.$$

Similarly, the reduced matrix elements for the electronic field gradient may be further reduced according to

$$\langle N', S', J'||T^{(2)}(\nabla \cdot \mathbf{E}_1)||N, S, J\rangle = \delta_{S',S}(-1)^{N'+S+J}[(2J+1)(2J'+1)]^{1/2} \begin{Bmatrix} N' & 2 & N \\ J & S & J' \end{Bmatrix} \langle N'||T^{(2)}(\nabla \cdot \mathbf{E}_1)||N\rangle.$$

It is convenient to write the electric-field gradient in terms of molecule-fixed components using rotation matrices, in order to express the N dependence of its reduced matrix elements explicitly:

$$T_p^{(2)}(\nabla \cdot \mathbf{E}_i) = \sum_q \mathcal{D}_{pq}^{(2)*}(\omega) T_q^{(2)}(\nabla \cdot \mathbf{E}_i),$$

where p refers to space-fixed axes, q to molecule-fixed axes, and ω represents the three Euler angles. For symmetric rotor wave functions $|N, K\rangle$ we have [32]

$$\langle N', K'||\mathcal{D}_{pq}^{(k)*}(\omega)||N, K\rangle = (-1)^{N'-K'}[(2N'+1)(2N+1)]^{1/2} \begin{pmatrix} N' & k & N \\ -K' & q & K \end{pmatrix}.$$

In our case we have $K=K'=0$, $k=2$. Combining the above relationships and introducing the standard definition of the electric-field gradient [25]

$$q = q_2 = q_1 \equiv \left\langle \frac{\partial^2 V}{\partial z^2} \right\rangle = 2\langle T_0^{(2)}(\nabla \cdot \mathbf{E}_1)\rangle,$$

where the expectation value is taken over the electronic state, we arrive at the complete matrix element given in Sec. IV.

* Permanent address: Department of Chemistry, Arizona State University, Tempe, AZ 85287.

† Present address: Communaissance, Box 422, Downers Grove, IL 60515

[1] A. Lofthus and P. H. Krupenie, J. Phys. Chem. Ref. Data **6**, 113 (1977).

[2] S. D. Rosner, T. D. Gaily, and R. A. Holt, Phys. Rev. A **26**, 697 (1982).

[3] S. D. Rosner, T. D. Gaily, and R. A. Holt, J. Mol. Spectrosc. **109**, 73 (1985).

[4] S. L. Kaufman, Opt. Commun. **17**, 309 (1976).

[5] This is because those transitions that satisfy $\Delta F=\Delta J=\Delta N$ (principal transitions) are more intense than those that do not (satellite transitions), and the intensities of the satellite lines decrease rapidly with N, the rotational angular momentum due to end-over-end tumbling. [See A. Sommerfeld and W. Heisenberg, Z. Phys. **11**, 131 (1922); G. Herzberg, *Molecular Spectra and Molecular Structure I: Spectra of Diatomic Molecules* (Van Nostrand, New York, 1950), p. 244.]

[6] R. C. Woods, in *Ion and Cluster Ion Spectroscopy and Structure*, edited by J. P. Maier (Elsevier, Amsterdam, 1989), p. 27.

[7] R. D. Brown, P. D. Godfrey, D. C. McGilvery, and J. G. Crofts, Chem. Phys. Lett. **84**, 437 (1981).

[8] M. A. Johnson, M. L. Alexander, I. Hertel, and W. C. Lineberger, Chem. Phys. Lett. **105**, 374 (1984).

[9] A. Carrington, I. R. McNab, and C. A. Montgomerie, Mol. Phys. **66**, 519 (1989); Chem. Phys. Lett. **160**, 237 (1989).

[10] A. Carrington, I. R. McNab, C. A. Montgomerie, and J. M. Brown, Mol. Phys. **66**, 711 (1989).

[11] L. Young, T. Dinneen, and N. B. Mansour, Phys. Rev. A **38**, 3812 (1988); A. Sen, L. S. Goodman, and W. J. Childs, Rev. Sci. Instrum. **59**, 74 (1988).

[12] S. D. Rosner, R. A. Holt, and T. D. Gaily, Phys. Rev. Lett. **35**, 785 (1975).

[13] W. Ertmer and B. Hofer, Z. Phys. A **276**, 9 (1976).

[14] W. J. Childs, O. Poulsen, and L. S. Goodman, Phys. Rev. A **19**, 160 (1979).

[15] A. Yokozeki and J. S. Muenter, J. Chem. Phys. **72**, 3796 (1980).

[16] U. Kötz, J. Kowalski, R. Neumann, S. Noehte, H. Suhr, and K. Winkler, Z. Phys. A **300**, 25 (1981).

[17] M. Van Hove, G. Borghs, P. De Bisschop, and R. E. Silverans, Z. Phys. A **321**, 215 (1985).

[18] N. B. Mansour, T. P. Dinneen, and L. Young, Phys. Rev. A **39**, 5762 (1989).

[19] T. P. Dinneen, N. Berrah Mansour, C. Kurtz, and L. Young, Phys. Rev. A **43**, 4824 (1991).

[20] T. J. Scholl, T. D. Gaily, R. A. Holt, and S. D. Rosner, Phys. Rev. A. **33**, 2396 (1986).

[21] S. D. Rosner, T. D. Gaily, and R. A. Holt, Phys. Rev. Lett. **40**, 851 (1978).

[22] Colutron Research Corp., 2321 Yarmouth, Boulder, CO 80301.

[23] G. Borghs, P. De Bisschop, J. Odeurs, R. E. Silverans, and M. Van Hove, Phys. Rev. A **31**, 1434 (1985).

[24] I. I. Rabi, J. R. Zacharias, S. Millman, and P. Kusch, Phys. Rev. **53**, 318 (1938).

[25] N. F. Ramsey, *Molecular Beams* (Oxford University Press, Oxford, 1956), Chap. V.

[26] R. A. Frosch and H. M. Foley, Phys. Rev. **88**, 1337 (1952).

[27] M. Broyer, J. Vigué, and J. C. Lehmann, J. Phys. (Paris) **39**, 591 (1978).

[28] F. Hund, Z. Phys. **42**, 93 (1927).

[29] J. H. Van Vleck, Phys. Rev. **33**, 467 (1929).

[30] R. S. Mulliken, Rev. Mod. Phys. **2**, 60 (1930).

[31] W. J. Childs, D. R. Cok, G. L. Goodman, and L. S. Goodman, J. Chem. Phys. **75**, 501 (1981).

[32] I. C. Bowater, J. M. Brown, and A. Carrington, Proc. R. Soc. London, Ser. A **333**, 265 (1973).
[33] R. S. Freund, T. A. Miller, D. De Santis, and A. Lurio, J. Chem. Phys. **53**, 2290 (1970).
[34] W. H. Press, B. P. Flannery, S. A. Teukolsky, and W. T. Vetterling, *Numerical Recipes* (Cambridge University Press, Cambridge, 1986), Chap. 14.
[35] Ch. Ryzlewicz, H. U. Schütze-Pahlmann, J. Hoeft, and T. Törring, Chem. Phys. **71**, 389 (1982).
[36] R. A. Gottscho, R. W. Field, K. A. Dick, and W. Benesch, J. Mol. Spectrosc. **74**, 435 (1979).
[37] T. A. Miller, T. Suzuki, and E. Hirota, J. Chem. Phys. **80**, 4671 (1984).
[38] L. B. Knight, J. M. Bostick, R. W. Woodward, and J. Steadman, J. Chem. Phys. **78**, 6415 (1983).
[39] T. A. Dixon and R. C. Woods, J. Chem. Phys. **67**, 3956 (1977).
[40] W. Weltner, Jr., *Magnetic Atoms and Molecules* (Van Nostrand Reinhold, New York, 1983).
[41] P. E. Cade, K. D. Sales, and A. C. Wahl, J. Chem. Phys. **44**, 1973 (1966).
[42] G. H. Fuller, J. Phys. Chem. Ref. Data **5**, 835 (1976).
[43] C. W. Bauschlicher, Jr., S. R. Langhoff, H. Partridge, and D. P. Chong, J. Chem. Phys. **89**, 2985 (1988).
[44] A. Andersen and E. W. Thulstrup, J. Phys. B **6**, L211 (1973).
[45] A. L. Roche and H. Lefebrve-Brion, Chem. Phys. Lett. **32**, 155 (1975).
[46] S. R. Langhoff and C. W. Bauschlicher, Jr., J. Chem. Phys. **88**, 329 (1988).
[47] F. Herman and S. Skillman, *Atomic Structure Calculations* (Prentice-Hall, Englewood Cliffs, NJ, 1963).
[48] L. B. Knight, Jr., A. Ligon, R. W. Woodward, D. Feller, and E. R. Davidson, J. Am. Chem. Soc. **107**, 2857 (1985).
[49] N. Marcuvitz, *Waveguide Handbook* (McGraw-Hill, New York, 1951).
[50] A. Messiah, *Quantum Mechanics* (Wiley, New York, 1962), Vol. II, Appendix C.